

Multiple Latent Space Mapping for Compressed Dark Image Enhancement

Yi Zeng, Zhengning Wang*, Yuxuan Liu, Tianjiao Zeng, Xuhang Liu,
Xinglong Luo, Shuaicheng Liu, Shuyuan Zhu, Bing Zeng *Fellow, IEEE*

Abstract—Dark image enhancement aims at converting dark images to normal-light images. Existing dark image enhancement methods take uncompressed dark images as inputs and achieve great performance. However, in practice, dark images are often compressed before storage or transmission over the Internet. Current methods get poor performance when processing compressed dark images. Artifacts hidden in the dark regions are amplified by current methods, which results in uncomfortable visual effects for observers. Based on this observation, this study aims at enhancing compressed dark images while avoiding compression artifacts amplification. Since texture details intertwine with compression artifacts in compressed dark images, detail enhancement and blocking artifacts suppression contradict each other in image space. Therefore, we handle the task in latent space. To this end, we propose a novel latent mapping network based on variational auto-encoder (VAE). Firstly, different from previous VAE-based methods with single-resolution features only, we exploit multiple latent spaces with multi-resolution features, to reduce the detail blur and improve image fidelity. Specifically, we train two multi-level VAEs to project compressed dark images and normal-light images into their latent spaces respectively. Secondly, we leverage a latent mapping network to transform features from compressed dark space to normal-light space. Specifically, since the degradation models of darkness and compression are different from each other, the latent mapping process is divided mapping into enlightening branch and deblocking branch. Comprehensive experiments demonstrate that the proposed method achieves state-of-the-art performance in compressed dark image enhancement.

Index Terms—image enhancement, image compression, variational auto-encoder, multiple latent space

I. INTRODUCTION

DARK image enhancement is a basic task in image processing that aims to convert a dark image to a normal-light image for better visual effects. Up till now, many efforts have been made for dark image enhancement. Retinex-based methods like [1], [2] estimate the illumination map to attain reflectance map, and regard reflectance map as the enhanced result. In recent years, numerous neural networks concerning illumination enhancement have been proposed. Deep learning methods [3], [4] enhance images by decomposing dark images into reflectance map and illumination map based on Retinex theory. Jiang *et al.* [5] adopts generative adversarial networks to make under-exposed images enlightening. These methods take uncompressed images as inputs and achieve great

Yi Zeng, Zhengning Wang Yuxuan Liu, Tianjiao Zeng, Xuhang Liu, Xinglong Luo, Shuaicheng Liu, Shuyuan Zhu, Bing Zeng are with the School of Information and Communication Engineering, University of Electronic Science and Technology of China, Cheng Du, China, 611731 e-mail: zhengning.wang@uestc.edu.cn

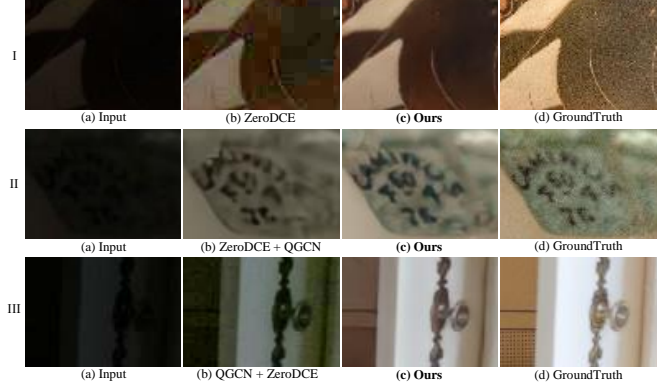


Fig. 1. Zoom-in details of the enhanced compressed dark image. (I-a, II-a, III-a) show the original images. (I-b) shows the comparative result with **enhancement** method. (II-b) shows the comparative result with the combination of the enhancement method and deblocking method (**enhancement+deblocking**). (III-b) shows the comparative result with the combination of deblocking method and enhancement method (**deblocking+enhancement**). ZeroDCE [6] is a enhancement method and QGCN [7] is a deblocking method.

performance. However, in actual applications, owing to the enormous data of the raw images, compression and encoding operation would be taken on images before transmission at the cost of information loss. Processing compressed images with existing dark image enhancement algorithms may amplify the compression blocking artifacts and causes poor visual effects, which is analyzed as following.

In the compression coding system such as JPEG which is based on discrete cosine transformation (DCT), the input image is partitioned into 8×8 encoding blocks and then DCT is implemented in each encoding block individually. The DCT coefficients will be quantized to reduce storage space. Such information loss weakens the correlation between different encoding blocks, causing discontinuities at the block boundaries. In the dark region, as texture details coupled with compression artifacts, existing dark image enhancement methods amplify the compression blocking artifacts hidden in the dark region, and amplify color distortion (adjacent encoding blocks expose the large difference in color), which is shown in Fig.1 (I.b). Although numerous approaches for compression artifacts suppression [7]–[10] have been developed, the discontinuity between neighbor blocks will be amplified dramatically and hard to smooth via post-processing. Fig.1 (II.b) shows the result of **enhancement+deblocking**, *i.e.*, performing the enhancement algorithm, and then the deblocking algorithm afterwards. Obviously, texture detail in Fig.1 (II.b) suffer

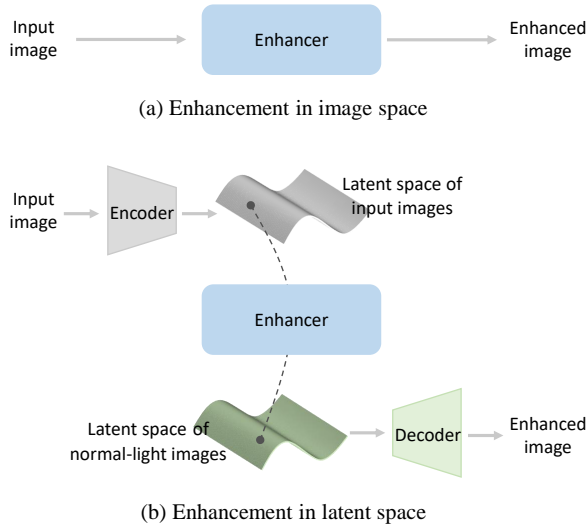


Fig. 2. **Conceptual comparison of two enhancement mechanisms.** Image space enhancement enhances from image to image directly, and latent space enhancement work through mapping points on manifolds.

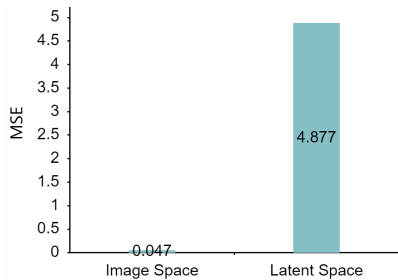


Fig. 3. **Mean Square Error (MSE) between compressed data and uncompressed data on dark face test dataset with 6000 dark images.**

from distortion. In addition, since the blocking artifacts are hard to perceive in dark compressed images, direct processing deblocking algorithms could result in blurred details. Fig.1 (III.b) shows the result of **deblocking+enhancement**, *i.e.*, performing the deblocking algorithm, and then the enhancement algorithm. It can be seen some blocking artifacts in Fig.1 (III.b) are still remained.

Most methods perform enhancement in image space, enhancing the dark images to enhanced results directly (shown in Fig.2 (a)). However, in compressed dark images, the blocking artifact is a type of detail. Since the texture detail intertwines with blocking artifacts, detail enhancement and blocking artifacts suppression contradict each other in image space. On the other hand, as data representation in latent space is denser than in image space [11], learning a mapping model in latent space is easier than in image space [12]. Besides, the difference between compressed dark and uncompressed dark images is too small, so that it is difficult for enhancer to discriminate the blocking artifacts hidden in compressed dark images. We argue that better discrimination between the compressed and uncompressed data is presented in latent space than in image space, and we found that Mean Square Error (MSE) between compressed data and uncompressed data is rise after projecting into latent space (0.047 *v.s.* 4.877) as illustrated in Fig.3.

Therefore, our approach takes the mapping from compressed dark images to normal-light images in latent space as shown in Fig.2 (b).

In this study, we propose a novel latent mapping network based on variational auto-encoder (VAE). Firstly, different from previous VAE-based methods which map with single-resolution features only, we propose to learn multiple latent spaces with multi-resolution features, to maintain detailed resolution information and improve semantic representation ability. Specifically, we train two multi-level VAEs to project compressed dark images and normal-light images into latent spaces respectively. Secondly, for each feature-level, we train a latent mapping network to transform features from compressed dark space to normal-light space, to learn the restoration from compressed dark images to normal-light images. For the latent space mapping, we divide it into two branches, *i.e.*, enlighten branch and deblocking branch, as the degradation models of darkness and compression are different from each other. Comprehensive experiments demonstrate that the proposed method achieves state-of-the-art performance in compressed dark image enhancement.

Our contributions are summarized as follows.

- We introduce the compressed dark image enhancement task that aims to enhance compressed dark images while avoiding amplifying the compression artifacts. We take this task as a mapping problem and propose mapping in latent space to reduce the difficulty of learning an enhancer.
- Our approach learns multiple latent spaces with multi-resolution features to reduce the detail blur and improve image fidelity.
- In this paper, we divide the latent space mapping into two branches, *i.e.*, enlighten branch and deblocking branch, as the degradation models of darkness and compression are different from each other.
- Comprehensive experiments demonstrate that the proposed method achieves state-of-the-art performance in compressed dark image enhancement.

II. RELATED WORK

A. Conventional Methods

Histogram equalization (HE) enhances the images by stretching the dynamic range. The variants of HE achieve some improvements, such as [13] can preserve the mean brightness of the input image. Another extension [14] stretches the dynamic range without making any loss of details in it. Wang *et. al.* [15] propose a fast and effective method by modifying weight and threshold. In the conventional field, one of the most widely employed methods is based on Retinex theory, which decomposes an image into reflectance map and the illumination map, and uses reflectance map as the final enhanced result. [16] estimates illumination by single-scale Gaussian blur. In [17], an exposure correction based on Retinex is introduced. Fu *et. al.* [18] estimates both the reflectance and the illumination by a weighted variational model. Guo *et. al.* [1] propose estimating illumination by imposing a structure prior to it. Methods [19], [20] pay attention to

noise suppression. Li *et al.* [19] introduces a robust Retinex model that considers a noise map, to improve the enhancement performance of low-light images accompanied by intensive noise. And Ren *et al.* [20] is based on the low-rank regularized Retinex Model, which is called LR3M, to suppress noise in the reflectance map.

B. Deep-learning Methods

In recent years, more researchers have focused on deep learning. Inspired by bilateral grid processing, Gharbi *et al.* [21] introduces a neural network architecture. In [22], a hybrid network with an encoder-decoder network and RNN was applied to improve image quality. Hu *et al.* [23] presents an automatic retouching system learning from unpaired data, by modeling retouching operations in a unified manner as resolution-independent differentiable filters. Methods [3], [4], [24], [25] construct their network based on Retinex theory. DRBN [26] recovers a linear band representation with paired images, and then recomposes the given bands via another learnable linear transformation with paired images, to extract a series of coarse-to-fine band representations with unpaired images. In [27], Xu *et al.* propose a frequency-based decomposition-enhancement model, which learns to recover image in the low-frequency layer and then enhances details in high-frequency. [28] repeatedly unfold the input image for feature extraction by a recursive unit that is composed of a recursive layer and a residual block. Xia *et al.* [29] introduce a neural network that applies the kernel field to the no-flash image, and then multiplies the result with the gain map to create the final output, to denoise low-light images. Different from the single image enhancement, [30] takes advantage of multi-exposure images to adjust brightness. Moseley *et al.* [31] present a denoising approach to enhance extremely low-light images of permanently shadowed regions (PSRs) on the lunar surface. Some researchers adopted generative adversarial networks for image enhancement processing, such as [5], [32], [33]. Guo *et al.* [6] propose a self-supervised approach for image enhancement, and this work formulates light enhancement as a task of image-specific curve estimation. [34] propose a structure-texture aware network, which is called STANet, to improve perceptual quality through successfully exploiting structure and texture features of low-light images. Ma *et al.* [35] develop a self-calibrated illumination learning framework, to realize a faster, more flexible, and more robust enhancement model. These approaches attain remarkable achievements in image enhancement, but most of them rely on high-quality images. Side effects such as blocking artifacts amplification arise when dealing with compressed image through these algorithms.

C. Artifacts Reduction

Blocking artifacts bring terrible visual effect to observers. To reduce blocking artifacts and obtain high-quality images, researchers have proposed many solutions. Various compression standard, *i.e.*, JPEG [36], JPEG2000 [37], H.264 [38], *etc.*, adopt deblocking filter in the decoder. The early work ARCNN [8] first adopts CNN to solve this problem, and

create a precedent for the CNN-based methods. In [39], image deblocking is modeled as an optimization problem within maximum a posteriori framework, and an algorithm that contains structural sparse representation (SSR) prior and quantization constraint (QC) prior is proposed for compression artifacts removal. [40] introduces a pseudo-blind system, which removes compression artifacts by estimating the quality factor and then applying a network that is trained with a similar quality factor. For JPEG image compression artifacts reduction, Jin *et al.* [41] propose a dual-stream recursive residual network (STRRN) which consists of structure and texture streams for separately reducing the specific artifacts related to high-frequency or low-frequency image components. Fu *et al.* [42] propose an interpretable deep network to learn both pixel-level regressive prior and semantic-level discriminative prior. In [9], a model-driven deep unfolding method is introduced to remove the artifacts. These methods are effective for compression artifacts reduction. However, compression artifacts are not easily perceived in low-light images. As a side effect of image enhancement processing, amplified artifacts along with color distortion are hard to be removed by the algorithms mentioned above.

III. THE PROPOSED METHOD

A. Overview

We define the compressed dark image space as \mathcal{C} and the normal-light image space as \mathcal{N} . Then, we define images sampled from these two spaces as $c \in \mathcal{C}$ and $n \in \mathcal{N}$. The enhancement can be established as a mapping from \mathcal{C} to \mathcal{N} . The proposed method is implemented in following steps.

First, the image spaces \mathcal{C} and \mathcal{N} are encoded into their latent spaces \mathcal{L}_C and \mathcal{L}_N respectively as:

$$\mathcal{L}_C = \mathcal{E}_C(\mathcal{C}), \quad \mathcal{L}_N = \mathcal{E}_N(\mathcal{N}) \quad (1)$$

where \mathcal{E}_C and \mathcal{E}_N denote the encoding operation for \mathcal{C} and \mathcal{N} respectively.

Second, we learn two decoders that reconstruct the input images from the latent features:

$$\mathcal{C} = \mathcal{D}_C(\mathcal{L}_C), \quad \mathcal{N} = \mathcal{D}_N(\mathcal{L}_N) \quad (2)$$

where \mathcal{D}_C and \mathcal{D}_N denote the decoders for \mathcal{L}_C and \mathcal{L}_N respectively.

Third, we perform enhancement in the latent spaces. Specifically, we learn the latent mapping from \mathcal{L}_C to \mathcal{L}_N as:

$$\mathcal{L}_N = \mathcal{M}(\mathcal{L}_C) \quad (3)$$

where \mathcal{M} is the latent mapping operation.

By learning such a latent mapping operation, the whole enhancement can be formulated as:

$$\mathcal{N} = \mathcal{D}_N(\mathcal{M}(\mathcal{E}_C(\mathcal{C}))) \quad (4)$$

Therefore, our approach consists of two stages: Firstly, we learn latent space \mathcal{L}_C and \mathcal{L}_N for compressed dark images and normal-light images respectively; Secondly, we learn latent space mapping function \mathcal{M} to transform features from \mathcal{L}_C to \mathcal{L}_N .

B. Expand to Multiple Latent Spaces

Low-resolution features are rich in semantic information, and high-resolution features are rich in detailed information. The current single-level mapping model is difficult to consider both. In order to get enhanced results with high fidelity and rich textures, we expand the latent space to multi-level. The intuition of the proposed multiple latent space mapping is shown in Fig. 4.

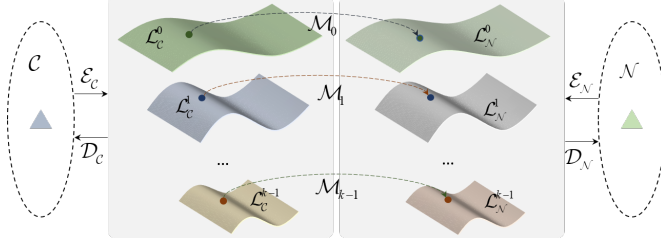


Fig. 4. Intuition of multiple latent space mapping.

First, we learn multiple latent spaces with multi-resolution latent features for \mathcal{C} and \mathcal{N} respectively. Therefore, Eq. 1 can be rewritten as:

$$\begin{aligned} \mathcal{L}_C^0, \mathcal{L}_C^1, \dots, \mathcal{L}_C^{k-1} &= \mathcal{E}_C(\mathcal{C}) \\ \mathcal{L}_N^0, \mathcal{L}_N^1, \dots, \mathcal{L}_N^{k-1} &= \mathcal{E}_N(\mathcal{N}) \end{aligned} \quad (5)$$

where \mathcal{E}_C and \mathcal{E}_N denote the encoding operation for \mathcal{C} and \mathcal{N} respectively, $\{\mathcal{L}_C^i\}_{i=0}^{k-1}$ and $\{\mathcal{L}_N^i\}_{i=0}^{k-1}$ are the encoded multiple latent spaces which include multi-resolution latent features for \mathcal{C} and \mathcal{N} respectively. The feature resolution of $\{\mathcal{L}_C^i\}_{i=0}^{k-1}$ is monotonically decreasing, so does $\{\mathcal{L}_N^i\}_{i=0}^{k-1}$.

Second, we learn two decoders that reconstruct the multi-resolution latent features to the input images. Therefore, Eq. 2 can be rewritten as:

$$\begin{aligned} \mathcal{C} &= \mathcal{D}_C(\mathcal{L}_C^0, \mathcal{L}_C^1, \dots, \mathcal{L}_C^{k-1}) \\ \mathcal{N} &= \mathcal{D}_N(\mathcal{L}_N^0, \mathcal{L}_N^1, \dots, \mathcal{L}_N^{k-1}) \end{aligned} \quad (6)$$

where \mathcal{D}_C and \mathcal{D}_N denote the decoders for $\{\mathcal{L}_C^i\}_{i=0}^{k-1}$ and $\{\mathcal{L}_N^i\}_{i=0}^{k-1}$ respectively.

Third, we learn multiple latent space mapping from $\{\mathcal{L}_C^i\}_{i=0}^{k-1}$ to $\{\mathcal{L}_N^i\}_{i=0}^{k-1}$. Therefore, Eq. 3 can be rewritten as:

$$\begin{aligned} \mathcal{L}_N^{k-1} &= \mathcal{M}_{k-1}(\mathcal{L}_C^{k-1}) \\ \mathcal{L}_N^{k-2} &= \mathcal{M}_{k-2}(\mathcal{L}_C^{k-2}) \\ &\dots \\ \mathcal{L}_N^0 &= \mathcal{M}_0(\mathcal{L}_C^0) \end{aligned} \quad (7)$$

Finally, enhancement towards multiple latent space mapping can be formulated as:

$$\mathcal{N} = \mathcal{D}_N(\{\mathcal{M}_0, \mathcal{M}_1, \dots, \mathcal{M}_{k-1}\}(\mathcal{E}_C(\mathcal{C}))) \quad (8)$$

Next, we introduce the details of these two parts in Section III-C and Section III-D respectively.

C. Learning Multiple Latent Spaces

Since variational auto-encoder (VAE) [43] encodes the input images to latent features with Gaussian distribution where the images can be reconstructed by sampling codes from

latent space, we propose to learn multiple latent spaces for compressed dark images and normal-light images respectively by training two multi-level VAEs.

1) **Intuition of Multi-level VAE:** The structure of our multi-level VAEs is shown in Fig. 5. For compressed dark images, firstly, we use a group of sub-encoders to encode the input image to latent features as:

$$\begin{aligned} l_c^0 &= \mathcal{E}_C^0(c) \\ l_c^1 &= \mathcal{E}_C^1(l_c^0 \downarrow) \\ &\dots \\ l_c^{k-1} &= \mathcal{E}_C^{k-1}(l_c^{k-1} \downarrow) \end{aligned} \quad (9)$$

where $\{l_c^i\}_{i=0}^{k-1}$ are the encoded latent features for the input compressed dark image c , $\{\mathcal{E}_C^i\}_{i=0}^{k-1}$ are the sub-encoders, and \downarrow means downsample by a factor of 2.

Then, we feed the encoded latent feature to a group of sub-decoders to reconstruct the input image as:

$$\begin{aligned} y_c^{k-2} &= \mathcal{D}_C^{k-1}(l_c^{k-1}) \uparrow + l_c^{k-2} \\ y_c^{k-3} &= \mathcal{D}_C^{k-2}(y_c^{k-2}) \uparrow + l_c^{k-3} \\ &\dots \\ \hat{c} &= \mathcal{D}_C^0(y_c^0) \end{aligned} \quad (10)$$

where \hat{c} is the reconstructed image of c , $\{\mathcal{D}_C^i\}_{i=0}^{k-1}$ are the sub-decoders, and \uparrow means upsample by a factor of 2.

Similarly, the reconstruction process for normal-light images is shown as:

$$\begin{aligned} \{l_n^i\}_{i=0}^{k-1} &= \{\mathcal{E}_N^i\}_{i=0}^{k-1}(n) \\ \hat{n} &= \{\mathcal{D}_N^i\}_{i=0}^{k-1}(\{l_n^i\}_{i=0}^{k-1}) \end{aligned} \quad (11)$$

where $\{l_n^i\}_{i=0}^{k-1}$ are latent features for the input normal-light image n , \hat{n} is the reconstructed image of n , $\{\mathcal{E}_N^i\}_{i=0}^{k-1}$ are the sub-encoders for n , $\{\mathcal{D}_N^i\}_{i=0}^{k-1}$ are the sub-decoders for $\{l_n^i\}_{i=0}^{k-1}$.

For realization, the sub-encoders $\{\mathcal{E}_C^i\}_{i=0}^{k-1}$ and $\{\mathcal{E}_N^i\}_{i=0}^{k-1}$ are realized by 3×3 convolution followed by instance normalization and ReLU. The downsampling operation is realized by convolution with stride 2, and upsampling operation is realized by bilinear interpolation with scale factor of 2.

2) **Multi-level VAE Training:** Our approach learns the multiple latent spaces with standard Gaussian distribution. During the training stage, the loss function of training VAE for compressed dark images is defined as:

$$\begin{aligned} L_{\text{VAE}_C}(c) &= \|\hat{c} - c\| + L_{\text{PL}}(\hat{c}, c) + L_{\text{VAE}_C, \text{GAN}}(\hat{c}) \\ &\quad + \sum_{i=0}^{k-1} \text{KL}(l_c^i, N(0, 1)) \end{aligned} \quad (12)$$

where $\{l_c^i\}_{i=0}^{k-1}$ are the multi-level latent features of the input image c , \hat{c} is the reconstruction of c , and $N(0, 1)$ denotes the standard Gaussian distribution. The first item penalizes the least absolute deviations between \hat{c} and c , which constrains the VAE to reconstruct the input image, so as to enforce latent features to capture the major cues of images. The second item is perceptual loss [44] that constrains the consistency of both high-level and low-level features. The third item is the least-square loss (LSGAN) [45], which encourages the VAE

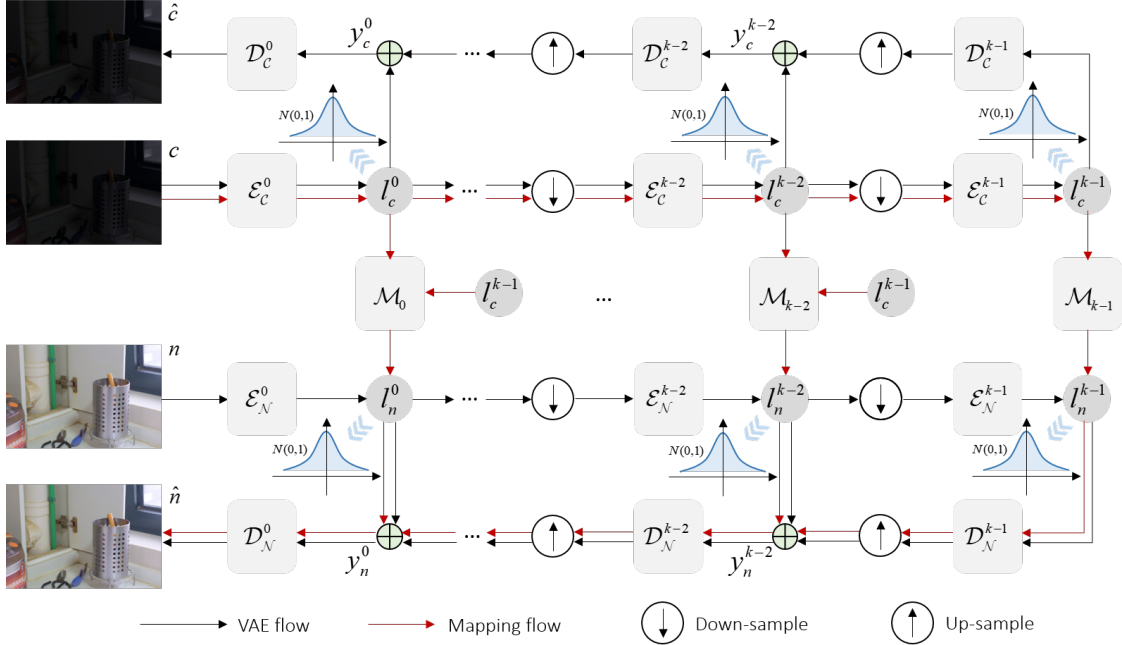


Fig. 5. Framework of the proposed multi-level VAEs and multiple latent space mapping.

Algorithm 1 Learning Multiple Latent Spaces

Require: Functions $\{\mathcal{E}_c^i\}_{i=0}^{k-1}$ and $\{\mathcal{D}_c^i\}_{i=0}^{k-1}$, c (batch of input images)

1) Encode with Eq. 9

For $i \in \{0, 1, \dots, k-1\}$:

if $i == 0$:

$$l_c^i \leftarrow \mathcal{E}_c^i(c)$$

else:

$$l_c^i \leftarrow \mathcal{E}_c^i(l_c^{i-1} \downarrow)$$

2) Decode with Eq. 10

For $i \in \{k-1, k-2, \dots, 1\}$:

if $i == k-1$:

$$y_c^{i-1} \leftarrow \mathcal{D}_c^i(l_c^i) \uparrow + l_c^{i-1}$$

else:

$$y_c^{i-1} \leftarrow \mathcal{D}_c^i(y_c^i) \uparrow + l_c^{i-1}$$

$$\hat{c} \leftarrow \mathcal{D}_c^0(y_c^0)$$

Loss Functions with Eq. 12

$$\theta \leftarrow \text{Update}(L_{\text{VAE}_c}(c))$$

Obtain latent features $\{l_c^i\}_{i=0}^{k-1}$ finally.

to reconstruct images with high realism. The fourth item is the KL-divergence that constrains the multi-level latent features to squeeze to the standard Gaussian distribution $N(0, 1)$.

Similar to Eq. 12, the loss function of training VAE_N can also be defined as:

$$L_{\text{VAE}_N}(n) = \|\hat{n} - n\| + L_{\text{PL}}(\hat{n}, n) + L_{\text{VAE}_N, \text{GAN}}(\hat{n}) + \sum_{i=0}^{k-1} \text{KL}(l_n^i, N(0, 1)) \quad (13)$$

D. Learning Latent Space Mapping

The multi-level latent features are obtained after training two VAEs for compressed dark images and normal-light images respectively. We propose to learn the image enhancement by learning multiple latent space mapping. Such a mapping manner brings the benefit in two folds: 1) the mapping in the low-dimensional latent space is easier than that in the high-dimensional image space, 2) the multiple mapping mechanism preserves multi-scale information, and reduces position and detail information blur caused by downsampling in current single-level mapping.

Algorithm 2 Learning Latent Space Mapping Network

Require: Functions $\{\mathcal{E}_c^i\}_{i=0}^{k-1}$, $\{\mathcal{E}_N^i\}_{i=0}^{k-1}$, $\{\mathcal{D}_N^i\}_{i=0}^{k-1}$, and $\{\mathcal{M}_i\}_{i=0}^{k-1}$, c (batch of compressed dark images), n (batch of normal-light images)

1) Encode c with Eq. 9

$$\{l_c^i\}_{i=0}^{k-1} \leftarrow \{\mathcal{E}_c^i\}_{i=0}^{k-1}(c)$$

2) Encode n with Eq. 9

$$\{l_n^i\}_{i=0}^{k-1} \leftarrow \{\mathcal{E}_N^i\}_{i=0}^{k-1}(n)$$

3) Map $\{l_c^i\}_{i=0}^{k-1}$ to $\{l_n^i\}_{i=0}^{k-1}$

For $i \in \{k-1, k-2, \dots, 0\}$:

$$\tilde{l}_n^i \leftarrow \mathcal{M}_i(l_c^i, l_c^{i-1} \uparrow)$$

4) Decode $\{\tilde{l}_n^i\}_{i=0}^{k-1}$ with Eq. 10

$$\tilde{n} \leftarrow \{\mathcal{D}_N^i\}_{i=0}^{k-1}(\{\tilde{l}_n^i\}_{i=0}^{k-1})$$

Training Stage

Freeze $\{\mathcal{E}_c^i\}_{i=0}^{k-1}$, $\{\mathcal{E}_N^i\}_{i=0}^{k-1}$ and $\{\mathcal{D}_N^i\}_{i=0}^{k-1}$

$$\theta \leftarrow \text{Update}(L_{\mathcal{M}}(n, \tilde{n}, \{l_n^i\}_{i=0}^{k-1}, \{\tilde{l}_n^i\}_{i=0}^{k-1}))$$

Inference Stage

Return \tilde{n}

1) Latent Space Mapping Network: Since the degradation models of darkness and compression are different from each

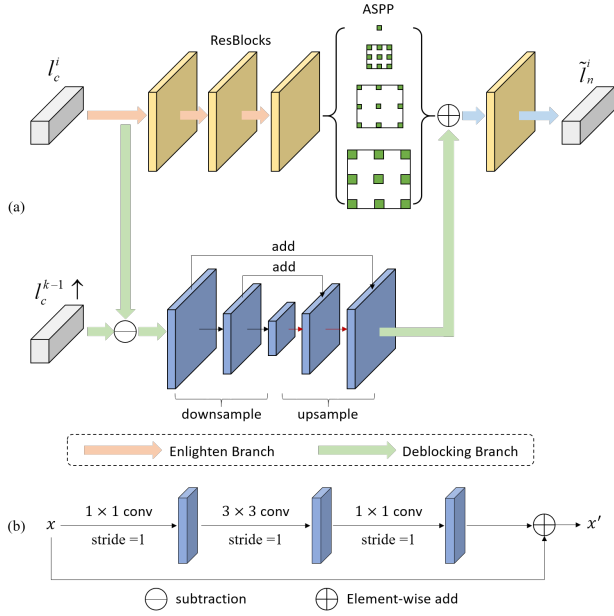


Fig. 6. **Structure of latent space mapping network.** (a) the major part of latent space mapping network. (b) the ResBlock in (a). l_c^i is the i -th level latent feature of compressed image. For enlighten branch, ASPP means Atrous Spatial Pyramid Pooling with different dilation rates as [1, 6, 12, 18]. For deblocking branch, the UNet-style network contains two downsample blocks and two upsample blocks. Each downsample block is realized by 3×3 convolution with stride of 2 and padding of 1. Each upsample block is realized by deconvolution layers with scale factor of 2.

other, we divide the latent space mapping into two branches, *i.e.*, enlighten branch and deblocking branch. Specifically, we design the latent mapping network as Fig. 6.

Enlighten Branch: Enlighten branch is used to restore the illumination cues and major details. Specifically, the enlighten branch takes the i -th latent feature l_c^i as input. It firstly enters into two ResBlocks (shown in Fig. 6 (b)). Then, the ASPP [46] (with dilation rate [1, 6, 12, 18]) is adopted to enhance the feature by aggregating multi-scale context cues. Finally, a ResBlock is leveraged to further enhance the feature with multi-scale context cues. The enlightening process is presented as:

$$F_{en} = f(l_c^i) \quad (14)$$

where F_{en} denotes the output of enlighten branch, $f(\cdot)$ means the learnable function of enlighten branch.

Deblocking Branch: Based on the fact that high-level features contain rich semantic cues and lack detail cues, we design the deblocking branch by considering the residual between l_c^i and top-level feature l_c^{k-1} , as l_c^{k-1} can be viewed as non-blocking feature (blocking artifact is a type of details). Therefore, the residual between l_c^i and l_c^{k-1} represents block-aware cues. Specifically, the deblocking branch firstly upsample l_c^{k-1} to the size of l_c^i as $l_c^{k-1} \uparrow$, and then compute the residual between l_c^i and $l_c^{k-1} \uparrow$. Then, a UNet-style network is adopted to remove the blocking artifact cues. The deblocking process is presented as:

$$F_{de} = g(l_c^i - l_c^{k-1} \uparrow) \quad (15)$$

where F_{de} denotes the output of deblocking branch, $g(\cdot)$ means the learnable function of deblocking branch.

Finally, the latent space mapping network performs element-wise add between the outputs of enlightening branch and deblocking branch, and feeds it into a ResBlock to obtain the mapping result \tilde{l}_n^i .

2) **Intuition of Latent Space Mapping:** Specifically, for the encoded latent features $\{l_c^i\}_{i=0}^{k-1}$, we propose to train k latent space mapping networks as:

$$\begin{aligned} \tilde{l}_n^{k-1} &= \mathcal{M}_{k-1}(l_c^{k-1}, l_c^{k-1} \uparrow) \\ \tilde{l}_n^{k-2} &= \mathcal{M}_{k-2}(l_c^{k-1}, l_c^{k-1} \uparrow) \\ &\dots \\ \tilde{l}_n^0 &= \mathcal{M}_0(l_c^0, l_c^{k-1} \uparrow) \end{aligned} \quad (16)$$

where $\{\tilde{l}_n^i\}_{i=0}^{k-1}$ are the predicted latent features for normal-light images whose ground-truths are $\{l_n^i\}_{i=0}^{k-1}$, and $\{\mathcal{M}_i\}_{i=0}^{k-1}$ are the mapping networks with the same structure.

Afterwards, the enhanced image \tilde{n} can be obtained by feeding $\{\tilde{l}_n^i\}_{i=0}^{k-1}$ into $\{\mathcal{D}_{\mathcal{N}}^i\}_{i=0}^{k-1}$ based on Eq. 10 as:

$$\begin{aligned} y_n^{k-2} &= \mathcal{D}_{\mathcal{N}}^{k-1}(\tilde{l}_n^{k-1}) \uparrow + l_n^{k-2} \\ y_n^{k-3} &= \mathcal{D}_{\mathcal{N}}^{k-2}(y_n^{k-2}) \uparrow + \tilde{l}_n^{k-3} \\ &\dots \\ \tilde{n} &= \mathcal{D}_{\mathcal{N}}^0(y_n^0) \end{aligned} \quad (17)$$

For convenient, we simplify Eq.17 to $\tilde{n} = \{\mathcal{D}_{\mathcal{N}}^i\}_{i=0}^{k-1}(\{\tilde{l}_n^i\}_{i=0}^{k-1})$.

For realization, the structure of the mapping network is shown in Fig. 6 (a). Firstly, l_c^i is taken into two residual blocks whose structure is shown in Fig. 6 (b). Then, channel attention and spatial attention are performed on the output of residual blocks. Finally, two residual blocks are taken to output the mapping latent feature \tilde{l}_n^i .

3) **Latent Space Mapping Training:** When training latent space mapping networks, the parameters of two VAEs are frozen, and only the parameters of mapping networks can be updated. The loss function of training the latent mapping networks is defined as:

$$L_{\mathcal{M}} = \sum_{i=0}^{k-1} \|\tilde{l}_n^i - l_n^i\| + L_{\text{PL}}(\tilde{n}, n) + L_{\text{LSGAN}}(\tilde{n}) \quad (18)$$

The first item penalizes the least absolute deviations between $\{\tilde{l}_n^i\}_{i=0}^{k-1}$ and $\{l_n^i\}_{i=0}^{k-1}$, which enforce the networks to learn the mapping between compressed dark domain and normal-light domain. The second item is perceptual loss that constrains the consistency of both high-level and low-level features, so as to further enforce the enhancer to learn the enhancement process. The third item is the least-square loss (LSGAN) [45] which encourages the ultimate enhancement results to look real.

4) **The Whole Enhancement:** After training two VAEs and the latent mapping networks, given a compressed dark image c , the enhancement result \tilde{n} can be obtained by:

$$\tilde{n} = \{\mathcal{D}_{\mathcal{N}}^i\}_{i=0}^{k-1} \circ \{\mathcal{M}_i\}_{i=0}^{k-1} \circ \{\mathcal{E}_{\mathcal{C}}^i\}_{i=0}^{k-1}(c) \quad (19)$$

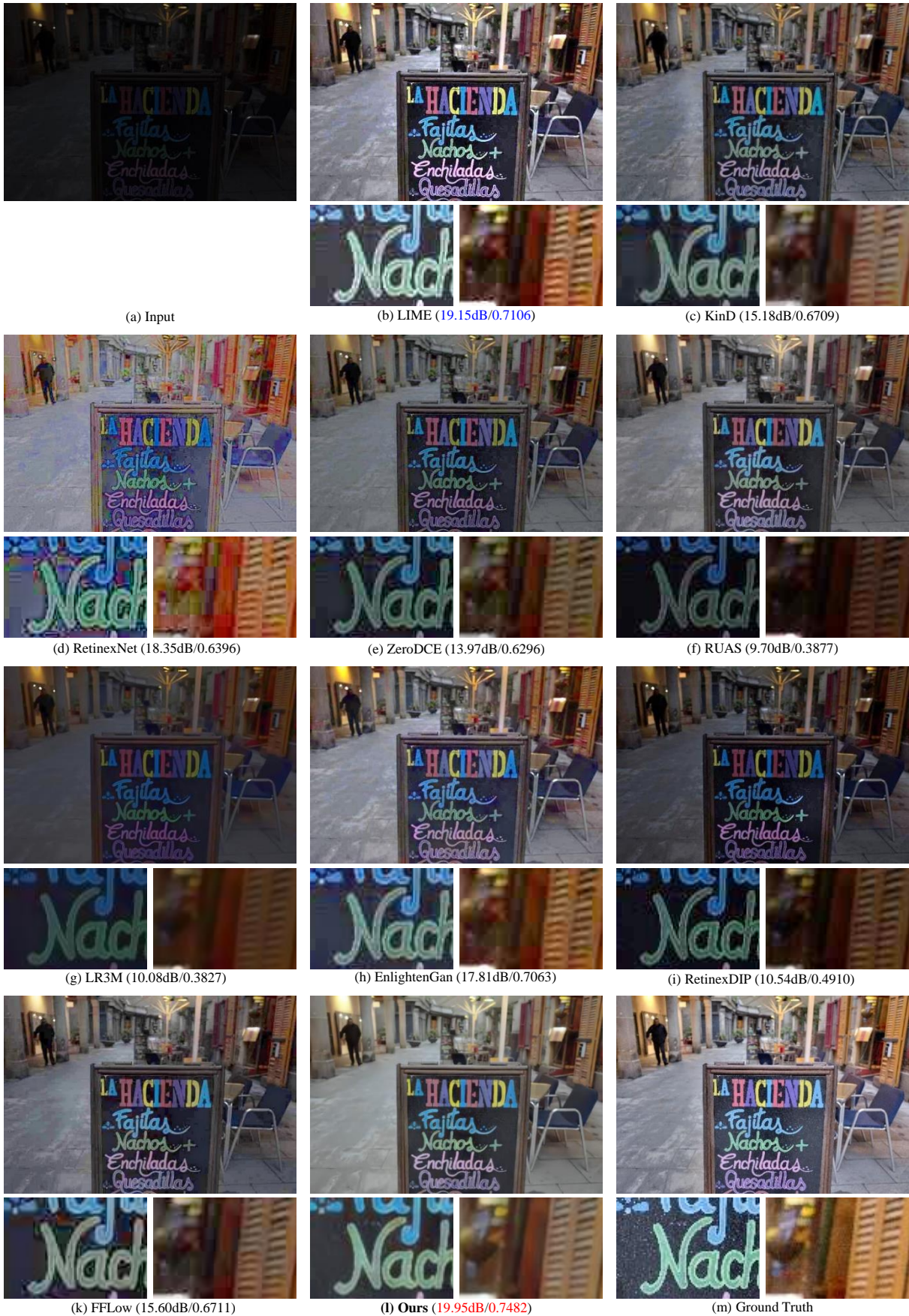


Fig. 7. Quantitative (PSNR/SSIM) and visual comparison with enhancement methods. The partial details are displayed with zoom-in. The best metrics are in red and the second best are in blue.

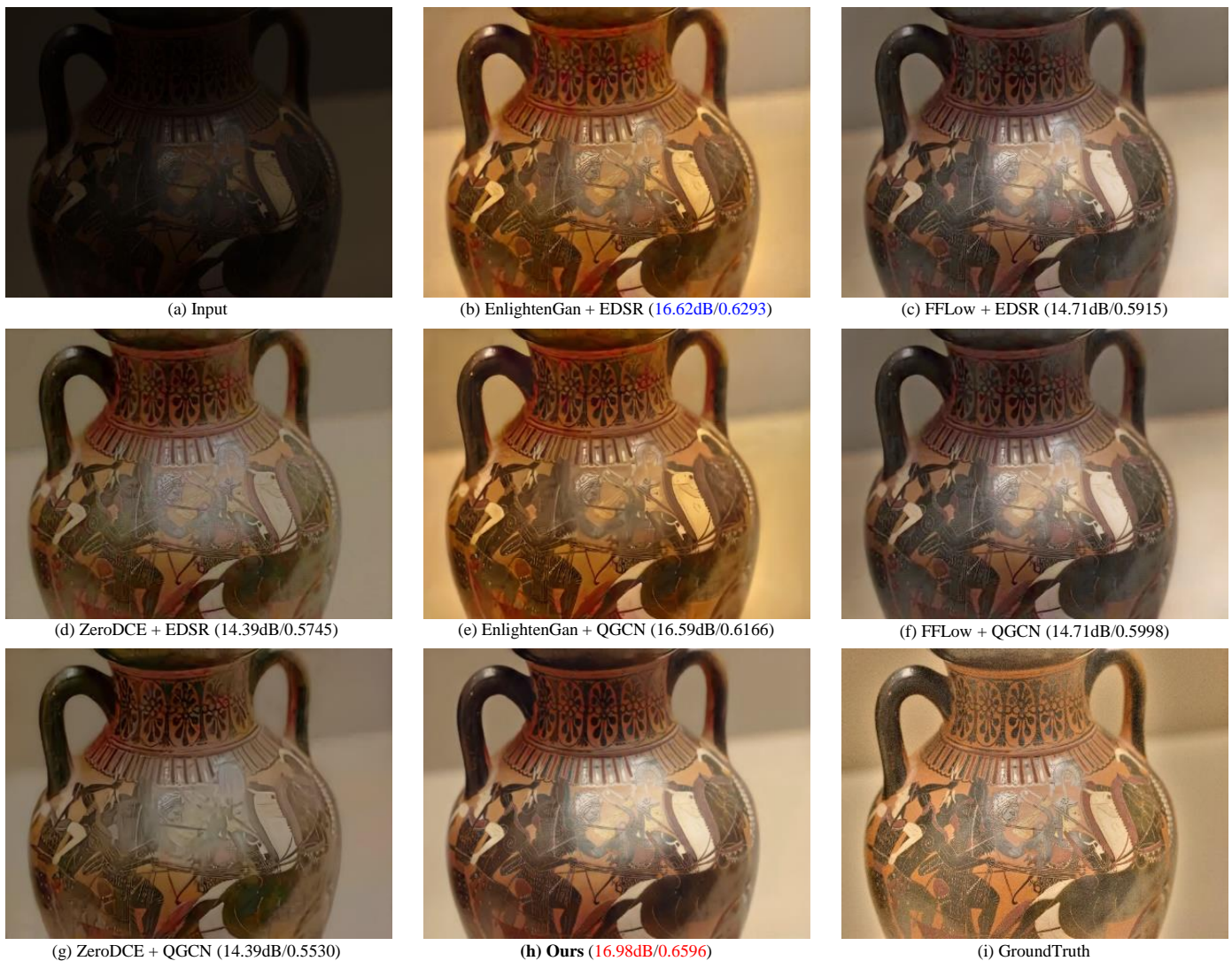


Fig. 8. **Quantitative (PSNR/SSIM) and visual comparison with enhancement+deblocking methods.** The best metrics are in red and the second best are in blue.

IV. EXPERIMENTS

A. Implementation Details

We implement the experiments on a Nvidia RTX 2080Ti GPU with PyTorch. We set the training batch size as 16. We utilize Adam optimizer for parameter learning. We set the start learning factor as 0.0002 and use linear learning factor decay. For each training iteration, we randomly crop patches of resolution 64×64 . Our training process contains two stages: VAE stage and mapping stage. Firstly, we train two VAEs with 1000 epochs. Secondly, we freeze the parameters of two VAEs and train the latent mapping network with 500 epochs. We adopt $k = 3$, *i.e.*, three-level latent space mapping, as the default setting.

B. Datasets

To improve the robustness of the model, we merge several real-world datasets captured from different scenarios.

1) *VAE Training Dataset*: We project dark images and normal-light images to latent spaces through two VAEs, re-

spectively. For the VAE of dark images, we collect 11831 dark images whose resources are exhibited in Table I. For the VAE of normal-light images, we use LabelME dataset [47] which contains 36417 normal-light images, containing indoor, street, and natural scenarios *et.al.*

TABLE I
THE RESOURCES OF 10831 DARK IMAGES FOR VAE. A7M3 MEANS PHOTOS TAKEN BY OURSELVES WITH SONY A7M3 CAMERA

Resource	Number	scenario
LOL [3]	485	furniture <i>et.al.</i>
LSRW [48]	5600	corridor, artificial constructions, food, dolls <i>et.al.</i>
SICE [30]	531	natural scenarios, artificial constructions <i>et.al.</i>
RELLISUR [49]	3605	papers with text, buildings, machinery <i>et.al.</i>
A7m3	610	office, buildings <i>et.al.</i>

2) *Mapping Training Dataset*: To train the latent mapping network, we collect 9923 image pairs whose resources are listed in Table II. Notely, since the dark images and reference images are misaligned in LSRW trainset and RELLSUR trainset, we adopt image registration algorithm [50] to align

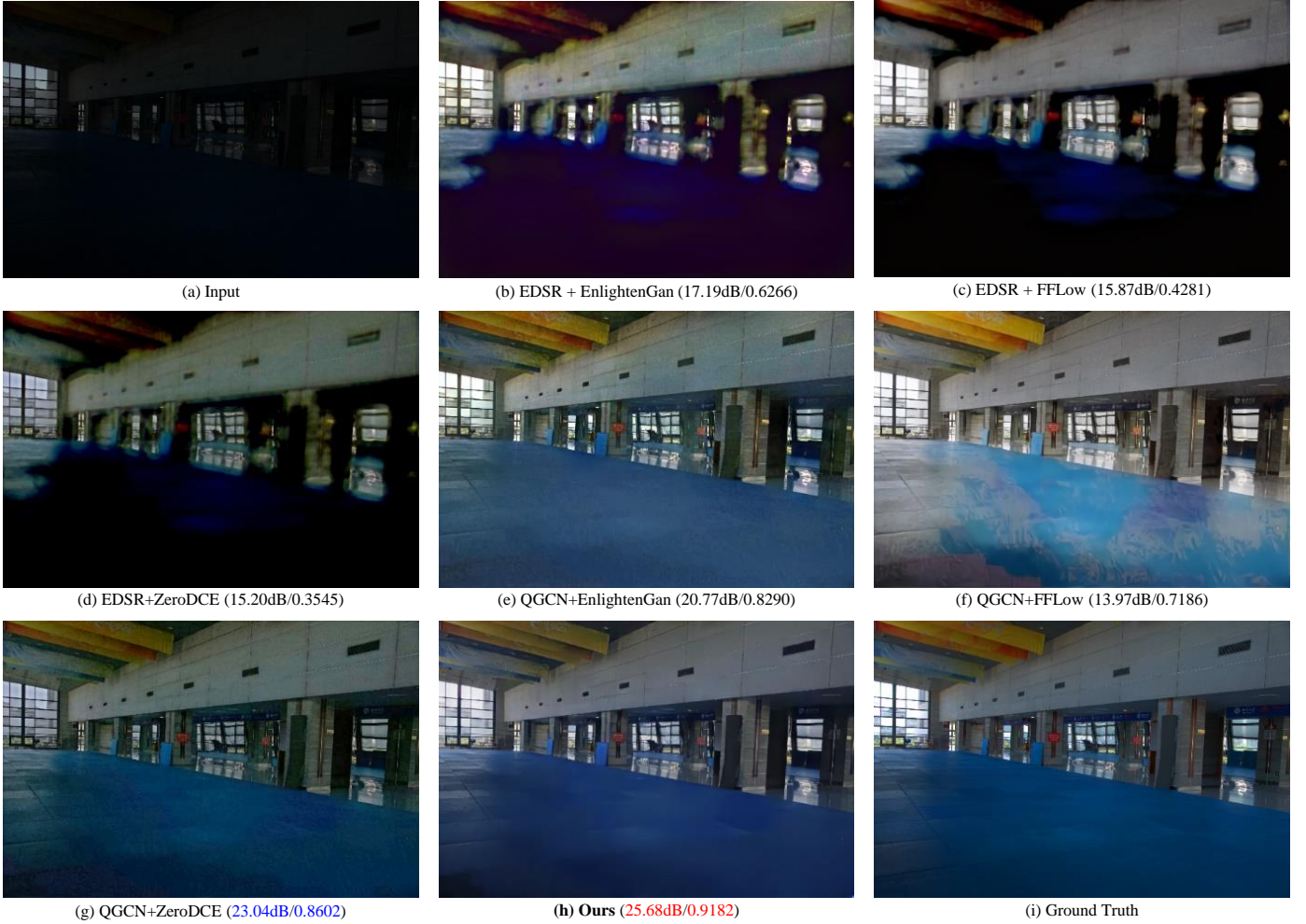


Fig. 9. **Quantitative (PSNR/SSIM) and visual comparison with deblocking+enhancement methods.** The best metrics are in red and the second best are in blue.

TABLE II

THE RESOURCES OF 9923 IMAGE PAIRS FOR MAPPING TRAINING DATASET. A7M3 MEANS PHOTOS TAKEN BY OURSELVES WITH SONY A7M3 CAMERA

Resource	Number	scenario
LOL [3]	485	furnitures <i>et.al.</i>
LSRW [48]	5260	corridor, artificial constructions, food, dolls <i>et.al.</i>
RELLISUR [49]	3568	papers with text, buildings, machinery <i>et.al.</i>
A7m3	610	office, buildings <i>et.al.</i>

them. Image pairs that fail to register are discarded.

3) *Test Dataset*: We use LOL testset, LSRW testset and SICE testset to test the performance of our approach.

C. Evaluation Metrics

Peak Signal-to-Noise Ratio (PSNR), Structure Similarity (SSIM) and PSNR-B [54] are widely used to evaluate the performance of compression artifacts reduction and light restoration. A higher PSNR value indicates a test image is closer to the reference image in terms of pixel-level image content. A higher SSIM value indicates a test image is closer to the reference image in terms of structural properties. PSNR-B is a block-sensitive image quality index designed to measure

the blocking artifacts, and a higher PSNR-B value indicates less blocking artifacts in test images.

D. Qualitative Evaluation

We present the visual comparisons on typical compressed dark images, and compare our approach with *i.e.*, **enhancement** methods, **enhancement+deblocking** methods and **deblocking+enhancement** methods.

1) *Compare with Enhancement Methods*: We show comparative visualization results in Fig. 7 to intuitively show performance. It is seen that most previous enhancement methods efficiently improve image brightness and contrast, but they amplify compression artifacts greatly; (g) avoids compression artifacts amplification but results in image details blur.

2) *Compare with Enhancement+Deblocking*: We further compare our approach with the manner processing outputs of enhancement algorithms with existing deblocking methods (**enhancement+deblocking**). After the joint processing of the enhancement algorithm and the deblocking algorithm, which is present in Fig. 8, the results obtained by the methods (b), (c), (d), (e), (f), (g) cause texture detail distortion. In contrast, the proposed method outperforms the existing methods in

TABLE III
 AVERAGE PSNR, SSIM AND PSNR-B OF ENHANCED RESULTS ON LOL TESTSET, LSRW TESTSET AND SICE DATASET WITH QFs 90%, 80%.
 THE BEST RESULTS ARE IN RED AND THE SECOND BEST ARE IN BLUE.

QF(%)	Method	LOL			LSRW			SICE		
		PSNR	SSIM	PSNR-B	PSNR	SSIM	PSNR-B	PSNR	SSIM	PSNR-B
90	LIME [1]	17.38	0.6353	17.16	14.89	0.4721	14.87	16.13	0.5030	16.25
	RetinexNet [3]	16.28	0.5925	16.29	14.03	0.4118	14.06	16.01	0.4734	16.07
	KinD [4]	16.98	0.6997	17.08	14.97	0.4362	15.03	16.16	0.4918	15.67
	EnlightenGAN [5]	17.81	0.7404	17.73	15.75	0.4071	15.56	16.11	0.5071	16.28
	RetinexDIP [51]	9.65	0.4316	9.76	11.74	0.2850	11.66	11.22	0.3507	11.60
	Zero-DCE [6]	15.67	0.6217	15.67	14.93	0.3946	15.35	14.81	0.4771	15.53
	LLFlow [52]	17.45	0.7633	17.59	15.38	0.4314	15.41	15.07	0.5004	15.63
	RUAS [25]	16.47	0.7271	16.41	12.12	0.4527	12.13	11.47	0.4271	11.41
	EnlightenGAN [5] + EDSR [53]	17.98	0.7747	17.99	15.95	0.4360	15.79	16.30	0.5131	16.31
	ZeroDCE [6] + EDSR [53]	15.87	0.6599	15.89	15.15	0.4213	15.64	14.93	0.4783	15.63
	LLFlow [52] + EDSR [53]	17.56	0.7884	17.70	15.53	0.4589	15.55	15.15	0.5048	15.62
	EnlightenGAN [5] + QGCN [7]	17.83	0.7918	17.88	16.07	0.4839	15.95	16.19	0.5021	16.40
	ZeroDCE [6] + QGCN [7]	16.92	0.7713	17.71	15.27	0.4805	15.82	14.92	0.4659	15.62
	LLFlow [52] + QGCN [7]	17.51	0.7855	17.69	15.46	0.4562	15.51	15.14	0.5070	15.72
	EDSR [53] + EnlightenGAN [5]	15.29	0.6311	15.67	15.68	0.4326	15.63	14.70	0.4703	14.87
	EDSR [53] + ZeroDCE [6]	12.61	0.5138	12.41	14.71	0.3785	14.99	13.55	0.4215	13.91
	EDSR [53] + LLFlow [52]	14.18	0.5689	14.01	14.49	0.4005	14.40	13.62	0.4367	14.00
	QGCN [7] + EnlightenGAN [5]	18.07	0.7985	17.97	15.91	0.4405	15.69	15.74	0.5373	15.73
	QGCN [7] + ZeroDCE [6]	14.97	0.7324	15.01	15.05	0.4340	15.48	14.66	0.5079	15.22
	QGCN [7] + LLFlow [52]	18.27	0.8113	18.25	15.32	0.4617	15.37	15.52	0.5452	16.08
Ours	19.16	0.8373	19.06	16.83	0.4959	16.81	16.20	0.5189	16.89	
80	LIME [1]	17.39	0.7035	17.21	14.43	0.3921	14.41	16.13	0.5118	16.21
	RetinexNet [3]	17.03	0.6734	16.84	13.44	0.3356	13.17	14.95	0.4625	14.98
	KinD [4]	17.20	0.7400	17.25	15.28	0.4392	15.34	15.16	0.5045	15.51
	EnlightenGAN [5]	18.03	0.7620	17.94	15.94	0.4447	15.74	15.98	0.5164	16.09
	RetinexDIP [51]	9.76	0.4188	10.16	12.59	0.3762	12.54	11.18	0.3549	11.57
	Zero-DCE [6]	14.99	0.7140	15.14	15.05	0.4409	15.46	14.73	0.4868	15.41
	LLFlow [52]	17.01	0.7606	17.28	15.28	0.4573	15.30	15.19	0.5158	15.72
	RUAS [25]	16.38	0.7195	16.25	13.76	0.3876	13.80	11.39	0.3710	12.15
	EnlightenGAN [5] + EDSR [53]	18.23	0.7802	18.27	16.13	0.4686	15.95	16.09	0.5235	16.14
	ZeroDCE [6] + EDSR [53]	15.04	0.7266	15.20	15.23	0.4653	15.71	14.86	0.4882	15.53
	LLFlow [52] + EDSR [53]	17.12	0.7910	17.43	15.41	0.4813	15.43	15.29	0.5212	15.72
	EnlightenGAN [5] + QGCN [7]	18.07	0.7888	18.06	16.15	0.4788	15.98	16.05	0.4977	16.18
	ZeroDCE [6] + QGCN [7]	14.92	0.7157	15.05	15.24	0.4727	15.78	14.85	0.4640	15.52
	LLFlow [52] + QGCN [7]	17.11	0.7864	17.45	15.32	0.4707	15.40	15.26	0.5217	15.80
	EDSR [53] + EnlightenGAN [5]	15.26	0.6298	15.61	15.66	0.4445	15.67	14.77	0.4627	14.94
	EDSR [53] + ZeroDCE [6]	12.56	0.5109	12.32	14.72	0.3875	15.00	13.52	0.4109	13.85
	EDSR [53] + LLFlow [52]	13.99	0.5647	13.83	14.42	0.4056	14.36	13.55	0.4277	13.93
	QGCN [7] + EnlightenGAN [5]	18.25	0.8124	18.21	15.93	0.4656	15.75	16.11	0.5297	16.01
	QGCN [7] + ZeroDCE [6]	14.99	0.7353	14.99	15.11	0.4612	15.56	14.77	0.4927	15.29
	QGCN [7] + LLFlow [52]	17.77	0.7985	17.86	15.14	0.4767	15.21	15.45	0.5249	16.06
Ours	18.92	0.8159	18.97	16.54	0.4947	16.51	16.59	0.5314	17.27	

brightness enhancement, detail texture restoration and block effect suppression, and achieves better results.

3) *Compare with **Deblocking+Enhancement***: We further compare our approach with the manner processing outputs of deblocking methods with existing enhancement algorithms (**deblocking+enhancement**). As shown in Fig.9, results of **deblocking+enhancement** still have blocking artifacts (e, f, g). In addition, such a manner even results in color distortion (b, c, d, f), which is caused by the fact that blocking artifacts in dark images are hard for deblocking models to perceive.

E. Quantitative Evaluation

In order to verify the effectiveness of our approach, we compare our approach with existing dark image enhancement methods with different quality factors (QF), *i.e.*, 90%, 80%, 70%, 60%. Table III show the comparison results with differ-

ent methods under QF 90% and 80%. The comparison results under QF 70% and 60% are listed in the appendix.

1) *Compare with **Enhancement Methods***: We compare our approach with one conventional methods, *i.e.*, LIME [1], and seven deep learning based methods, *i.e.*, RetinexNet [3], RetinexDIP [51], Kind [4], EnlightenGAN [5], ZeroDCE [6], LLFlow [52] and RUAS [25]. It can be seen that our approach is superior to the enhancement methods under different evaluation metrics.

2) *Compare with **Enhancement+Deblocking***: We further compare our approach with **enhancement+deblocking** methods. For LOL and LSRW datasets, our approach outperforms **enhancement+deblocking** methods under both full-referenced and no-referenced metrics. For SICE datasets, our approach outperforms **enhancement+deblocking** methods under PSNR and PSNR-B. For SSIM, our approach also achieves comparable performance.

TABLE IV
AVERAGE PSNR, SSIM AND PSNR-B AND OF ENHANCED RESULTS ON LOL TESTSET, LSRW TESTSET AND SICE DATASET WITH QFs 70%, 60%. THE BEST RESULTS ARE IN RED AND THE SECOND BEST ARE IN BLUE.

QF(%)	Method	LOL			LSRW			SICE		
		PSNR	SSIM	PSNR-B	PSNR	SSIM	PSNR-B	PSNR	SSIM	PSNR-B
70	LIME [1]	17.42	0.7089	17.35	14.46	0.4044	14.43	16.12	0.5030	16.28
	RetinexNet [3]	17.09	0.6828	16.96	13.48	0.3491	13.26	14.91	0.4503	15.01
	KinD [4]	17.28	0.7319	17.26	15.24	0.4427	15.27	15.08	0.4913	15.45
	EnlightenGAN [5]	18.21	0.7585	18.22	15.94	0.4505	15.73	15.12	0.5061	15.33
	RetinexDIP [51]	9.24	0.3972	9.58	12.62	0.3872	12.61	11.20	0.3524	11.60
	Zero-DCE [6]	15.04	0.7108	15.27	15.09	0.4490	15.50	14.80	0.4794	15.54
	LLFlow [52]	16.90	0.7519	17.23	15.25	0.4609	15.27	15.10	0.5015	15.67
	RUAS [25]	16.39	0.7136	16.36	13.80	0.3938	13.84	11.40	0.3669	12.20
	EnlightenGAN [5] + EDSR [53]	18.44	0.7868	18.25	16.11	0.4745	15.93	15.22	0.5139	15.38
	ZeroDCE [6] + EDSR [53]	15.10	0.7269	15.32	15.26	0.4736	15.73	14.91	0.4796	15.64
	LLFlow [52] + EDSR [53]	17.03	0.7844	17.40	15.37	0.4854	15.38	15.19	0.5075	15.67
	EnlightenGAN [5] + QGCN [7]	18.29	0.7812	18.31	16.07	0.4744	15.92	15.23	0.5067	15.48
	ZeroDCE [6] + QGCN [7]	15.04	0.7234	15.28	15.23	0.4724	15.77	14.93	0.4729	15.66
	LLFlow [52] + QGCN [7]	17.00	0.7731	17.39	15.28	0.4707	15.35	15.18	0.5095	15.77
	EDSR [53] + EnlightenGAN [5]	15.36	0.6282	15.84	15.67	0.4477	15.69	14.82	0.4572	15.04
	EDSR [53] + ZeroDCE [6]	12.63	0.5106	12.44	14.74	0.3904	15.03	13.55	0.4059	13.91
	EDSR [53] + LLFlow [52]	13.93	0.5615	13.82	14.42	0.4078	14.36	13.52	0.4219	13.94
	QGCN [7] + EnlightenGAN [5]	18.41	0.8097	18.29	15.90	0.4727	15.72	16.28	0.5198	16.32
	QGCN [7] + ZeroDCE [6]	15.09	0.7331	15.21	15.16	0.4683	15.61	14.86	0.4848	15.47
	QGCN [7] + LLFlow [52]	17.64	0.7990	17.84	15.15	0.4832	15.19	15.42	0.5144	16.07
Ours	18.46	0.7991	18.32	16.86	0.4982	16.86	15.90	0.5073	16.68	
60	LIME [1]	17.20	0.6939	17.00	14.45	0.4075	14.39	15.82	0.4853	15.78
	RetinexNet [3]	16.76	0.6750	16.63	13.45	0.3559	13.19	14.58	0.4388	14.52
	KinD [4]	17.15	0.7160	16.99	15.21	0.4411	15.27	14.76	0.4734	14.90
	EnlightenGAN [5]	18.13	0.7450	18.13	15.78	0.4514	15.54	15.05	0.4962	15.02
	RetinexDIP [51]	9.72	0.4250	10.03	12.58	0.3868	12.50	11.08	0.3351	11.46
	Zero-DCE [6]	14.94	0.6942	15.05	15.05	0.4473	15.45	14.78	0.4650	15.36
	LLFlow [52]	16.74	0.7343	17.12	15.17	0.4587	15.17	15.08	0.4865	15.60
	RUAS [25]	16.19	0.7006	15.97	13.79	0.3932	13.83	11.40	0.3601	12.14
	EnlightenGAN [5] + EDSR [53]	18.44	0.7778	18.61	15.96	0.4774	15.76	15.15	0.5048	15.07
	ZeroDCE [6] + EDSR [53]	15.00	0.7092	15.14	15.23	0.4706	15.70	14.88	0.4664	15.45
	LLFlow [52] + EDSR [53]	16.90	0.7716	17.35	15.31	0.4856	15.31	15.18	0.4943	15.62
	EnlightenGAN [5] + QGCN [7]	18.34	0.7811	18.37	15.90	0.4738	15.72	15.20	0.5055	15.27
	ZeroDCE [6] + QGCN [7]	15.08	0.7170	15.33	15.15	0.4684	15.62	14.92	0.4673	15.60
	LLFlow [52] + QGCN [7]	16.83	0.7520	17.27	15.22	0.4690	15.26	15.17	0.4949	15.71
	EDSR [53] + EnlightenGAN [5]	15.27	0.6209	15.58	15.53	0.4474	15.54	14.73	0.4519	14.83
	EDSR [53] + ZeroDCE [6]	12.56	0.5030	12.30	14.70	0.3886	14.99	13.53	0.3999	13.81
	EDSR [53] + LLFlow [52]	17.38	0.7737	17.65	15.19	0.4827	15.24	15.33	0.4987	15.93
	QGCN [7] + EnlightenGAN [5]	18.33	0.7970	18.42	15.75	0.4755	15.53	16.19	0.5112	16.02
	QGCN [7] + ZeroDCE [6]	15.00	0.7158	15.03	15.15	0.4673	15.63	14.85	0.4718	15.32
	QGCN [7] + LLFlow [52]	17.38	0.7737	17.65	15.19	0.4827	15.24	15.33	0.4987	15.93
Ours	18.65	0.7901	18.46	17.12	0.4966	17.05	16.45	0.4992	17.01	

3) *Compare with **Deblocking+Enhancement***: In addition, we compare our approach with **deblocking+enhancement** methods. For LOL dataset, when QF is set as 90% and 80%, our approach outperforms **deblocking+enhancement** methods. For LSRW dataset, our approach outperforms **deblocking+enhancement** methods. For SICE dataset, our approach still achieves comparable performance.

F. Ablation Studies

To verify the effectiveness of our proposed Multiple Latent Space Mapping method, we perform ablation studies from two perspectives. Firstly, we remove the latent mapping network and only train an encoder-decoder network to learn the enhancement. Secondly, we compare the performance of our latent mapping method with different levels, *i.e.*, single-level, two-level and three-level.

1) *Ablation for Latent Mapping Network*: We remove the latent mapping network \mathcal{M} to perform this ablation study. Specifically, we train an enhancement model with the same network structure as VAE, to learn the image restoration from compressed dark images to normal-light images directly. In this ablation study, we use LOL, LSRW and SICE datasets with QF 90%, and adopt PSNR, SSIM, PSNR-B as quantitative evaluation metrics. Table V displays the quantitative results for ablation of latent mapping network. It can be seen that the latent mapping network brings a large performance improvement.

2) *Ablation for Multiple Latent Spaces*: In order to verify the effectiveness of our multiple latent space mapping, we perform ablation studies for the mapping levels. Specifically, we test the performance under single-level latent space mapping (only mapping on the top level), two-level latent space mapping (mapping on the top and middle levels) and three-

TABLE V
QUANTITATIVE RESULTS FOR ABLATION OF LATENT MAPPING NETWORK

Dataset	\mathcal{M}	PSNR	SSIM	PSNR-B
LOL	✓	16.52	0.6729	16.57
		19.16	0.8373	19.06
LSRW	✓	15.07	0.4267	15.02
		16.83	0.4959	16.81
SICE	✓	15.89	0.4626	15.97
		16.20	0.5189	16.89

level latent space mapping (mapping on the top, middle and bottom levels) respectively. In this ablation study, we use LOL, LSRW and SICE dataset with QF 90%, and adopt PSNR, SSIM, PSNR-B as quantitative evaluation metrics.

TABLE VI
QUANTITATIVE RESULTS FOR ABLATION OF MULTIPLE LATENT SPACES

Dataset	Mapping level	PSNR	SSIM	PSNR-B
LOL	single-level	18.65	0.8097	19.23
	two-level	19.07	0.8146	19.49
	three-level	19.16	0.8373	19.06
LSRW	single-level	16.42	0.4856	16.42
	two-level	15.95	0.4830	16.01
	three-level	16.83	0.4959	16.81
SICE	single-level	15.98	0.5104	16.16
	two-level	16.12	0.5090	16.55
	three-level	16.20	0.5189	16.89

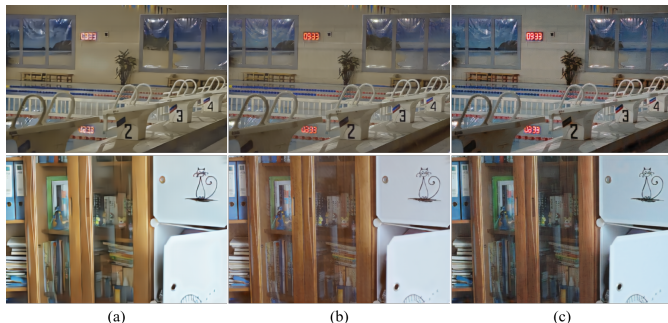


Fig. 10. Ablation study of multiple mapping. (a) results of single-level mapping. (b) results of two-level mapping. (c) results of three-level mapping.

The qualitative results of different levels are provided in Fig. 10. The single-level latent space mapping success to suppress the blocking artifacts, but results in image details blur and slight color distortion. Contrast to single-level, the two-level latent space mapping obtains better restoration results, but still causes color distortion. The three-level latent space mapping achieves great performance on details and color restoration with blocking artifacts suppression.

The quantitative results of different levels are provided in Table VI. It can be seen that three-level latent space mapping achieves the best PSNR and SSIM values, which is because the details are largely preserved by three-level latent space mapping. In LOL dataset, two-level latent space mapping achieves the best PSNR-B value, which is because two-level latent space mapping balances detail texture restoration and

TABLE VII
MAP ON DARK FACE WITH QF 90%. THE BEST VALUES ARE IN RED. THE SECOND BEST VALUES ARE IN BLUE.

Method	IoU threshold		
	0.3	0.5	0.7
LIME [1]	0.188049	0.169873	0.045380
RetinexNet [3]	0.147633	0.136992	0.039964
KinD [4]	0.159096	0.145566	0.042016
EnlightenGAN [5]	0.129158	0.120389	0.032258
RetinexDIP [51]	0.182877	0.165881	0.043670
Zero-DCE [6]	0.170194	0.156849	0.040050
LLFlow [52]	0.184419	0.169579	0.051443
RUAS [25]	0.169371	0.155320	0.042214
EnlightenGAN [5] + EDSR [53]	0.074730	0.070601	0.018611
ZeroDCE [6] + EDSR [53]	0.188670	0.172673	0.048338
LLFlow [52] + EDSR [53]	0.160536	0.149057	0.046590
EnlightenGAN [5] + QGCN [7]	0.039802	0.038792	0.009800
ZeroDCE [6] + QGCN [7]	0.108781	0.102474	0.030173
LLFlow [52] + QGCN [7]	0.183001	0.168877	0.050879
EDSR [53] + EnlightenGAN [5]	0.077944	0.073587	0.020028
EDSR [53] + ZeroDCE [6]	0.082400	0.077467	0.022322
EDSR [53] + LLFlow [52]	0.076276	0.072593	0.021737
QGCN [7] + EnlightenGAN [5]	0.186228	0.172047	0.048554
QGCN [7] + ZeroDCE [6]	0.193952	0.177015	0.047839
QGCN [7] + LLFlow [52]	0.179730	0.167152	0.052284
Ours	0.201467	0.185907	0.052263

blocking artifacts suppression. One could choose different mapping levels according to the specific requirements on detail texture restoration and blocking artifacts suppression.

G. Dark Face Detection

To further verify the effectiveness of our compressed dark image enhancement method, we test the performance of dark image enhancement methods on the face detection task under compressed dark conditions. Specifically, we use the DARK FACE dataset that composes 10000 images taken in the dark. Since the bounding boxes of test set are not publicly available, we use the training and validation sets, which totally contain 6000 images. We use PyramidBox [55] trained on WIDER FACE dataset [56] as the face detector. For the dark face detection, we first use dark image enhancers to restore the compressed dark images, and then use PyramidBox to get the detection results.

Table VII shows the comparisons of mean Average Precision (mAP) under different IoU thresholds (0.3, 0.5, 0.7). Under the IoU thresholds of 0.3 and 0.5, our approach achieves the best mAP value among different methods. When the IoU threshold is set to 0.9, the mAP values of different methods get poor, and our approach still achieves comparable performance.

We further present the comparisons of precision-recall (P-R) curves under IoU threshold 0.5 in Fig. 12. It can be seen that our approach performs better in the high recall range.

Fig.12 exhibits some visual examples of current methods and our approach. As all known, blocking artifacts are not friendly to long-distance tiny face detection. Our method performs better on long-distance tiny face detection because our method focuses on preserving details and removing blocking artifacts. Experiments of dark face detection further show the effectiveness of our approach.

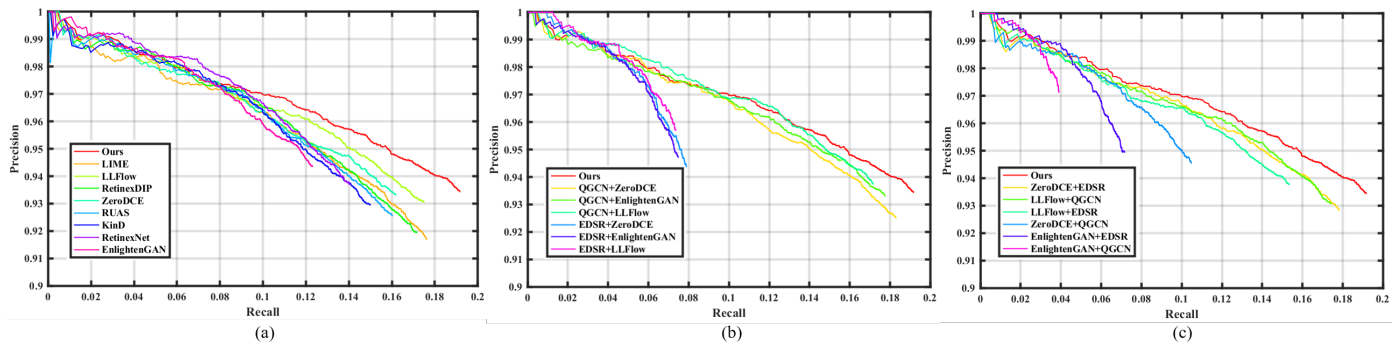


Fig. 11. P-R curve comparisons on dark face detection. (a) Comparisons with **enhancement** methods; (b) Comparisons with **enhancement+deblocking** methods; (c) Comparisons with **deblocking+enhancement** methods.



Fig. 12. Visualization of dark face detection. (a) Inputs; (b) ZeroDCE; (c) ZeroDCE+EDSR; (d) QGCN+ZeroDCE; (e) Ours.

V. CONCLUSION

We propose a significant task named compressed dark image enhancement and propose a novel method for this task. We have observed that compression artifacts would be enhanced by existing dark enhancement methods. Based on the observation, we propose to perform the restoration from compressed dark images to normal-light images in latent space. Specifically, we propose a novel two-branch latent mapping network based on multi-level VAE. Comprehensive experiments show the effectiveness of our approach. Furthermore, we perform experiments under different quality factors and show that our performance is comparable to existing methods.

REFERENCES

- [1] X. Guo, Y. Li, and H. Ling, "Lime: Low-light image enhancement via illumination map estimation," *IEEE Transactions on Image Processing*, vol. 26, no. 2, pp. 982–993, 2016.
- [2] P. Zhuang, C. Li, and J. Wu, "Bayesian retinex underwater image enhancement," *Engineering Applications of Artificial Intelligence*, vol. 101, p. 104171, 2021.
- [3] C. Wei, W. Wang, W. Yang, and J. Liu, "Deep retinex decomposition for low-light enhancement," in *Proceedings of British Machine Vision Conference*, 2018.
- [4] Y. Zhang, J. Zhang, and X. Guo, "Kindling the darkness: A practical low-light image enhancer," in *Proceedings of the 27th ACM international conference on multimedia*, 2019, pp. 1632–1640.
- [5] Y. Jiang, X. Gong, D. Liu, Y. Cheng, C. Fang, X. Shen, J. Yang, P. Zhou, and Z. Wang, "Enlightengan: Deep light enhancement without paired supervision," *IEEE Transactions on Image Processing*, vol. 30, pp. 2340–2349, 2021.
- [6] C. Guo, C. Li, J. Guo, C. C. Loy, J. Hou, S. Kwong, and R. Cong, "Zero-reference deep curve estimation for low-light image enhancement," in *Proceedings of the IEEE/CVF Conference on Computer Vision and Pattern Recognition*, 2020, pp. 1780–1789.
- [7] J. Li, Y. Wang, H. Xie, and K.-K. Ma, "Learning a single model with a wide range of quality factors for jpeg image artifacts removal," *IEEE Transactions on Image Processing*, vol. 29, pp. 8842–8854, 2020.
- [8] C. Dong, Y. Deng, C. C. Loy, and X. Tang, "Compression artifacts reduction by a deep convolutional network," in *Proceedings of the IEEE International Conference on Computer Vision*, 2015, pp. 576–584.
- [9] X. Fu, M. Wang, X. Cao, X. Ding, and Z.-J. Zha, "A model-driven deep unfolding method for jpeg artifacts removal," *IEEE Transactions on Neural Networks and Learning Systems*, 2021.
- [10] M.-H. Lin, C.-H. Yeh, C.-H. Lin, C.-H. Huang, and L.-W. Kang, "Deep multi-scale residual learning-based blocking artifacts reduction for compressed images," in *Proceedings of IEEE International Conference on Artificial Intelligence Circuits and Systems*. IEEE, 2019, pp. 18–19.
- [11] S. Gopalakrishnan, P. R. Singh, Y. Yazici, C.-S. Foo, V. Chandrasekhar, and A. Ambikapathi, "Classify and generate: Using classification latent space representations for image generations," *Neurocomputing*, vol. 471, pp. 296–334, 2022.

- [12] Z. Wan, B. Zhang, D. Chen, P. Zhang, D. Chen, J. Liao, and F. Wen, "Bringing old photos back to life," in *Proceedings of the IEEE/CVF Conference on Computer Vision and Pattern Recognition*, 2020, pp. 2747–2757.
- [13] H. Ibrahim and N. S. P. Kong, "Brightness preserving dynamic histogram equalization for image contrast enhancement," *IEEE Transactions on Consumer Electronics*, vol. 53, no. 4, pp. 1752–1758, 2007.
- [14] M. Abdullah-Al-Wadud, M. H. Kabir, M. A. A. Dewan, and O. Chae, "A dynamic histogram equalization for image contrast enhancement," *IEEE Transactions on Consumer Electronics*, vol. 53, no. 2, pp. 593–600, 2007.
- [15] Q. Wang and R. K. Ward, "Fast image/video contrast enhancement based on weighted thresholded histogram equalization," *IEEE Transactions on Consumer Electronics*, vol. 53, no. 2, pp. 757–764, 2007.
- [16] D. J. Jobson, Z.-u. Rahman, and G. A. Woodell, "Properties and performance of a center/surround retinex," *IEEE Transactions on Image Processing*, vol. 6, no. 3, pp. 451–462, 1997.
- [17] Q. Zhang, G. Yuan, C. Xiao, L. Zhu, and W.-S. Zheng, "High-quality exposure correction of underexposed photos," in *Proceedings of the 26th ACM international conference on Multimedia*, 2018, pp. 582–590.
- [18] X. Fu, D. Zeng, Y. Huang, X.-P. Zhang, and X. Ding, "A weighted variational model for simultaneous reflectance and illumination estimation," in *Proceedings of the IEEE Conference on Computer Vision and Pattern Recognition*, 2016, pp. 2782–2790.
- [19] M. Li, J. Liu, W. Yang, X. Sun, and Z. Guo, "Structure-revealing low-light image enhancement via robust retinex model," *IEEE Transactions on Image Processing*, vol. 27, no. 6, pp. 2828–2841, 2018.
- [20] X. Ren, W. Yang, W.-H. Cheng, and J. Liu, "Lr3m: Robust low-light enhancement via low-rank regularized retinex model," *IEEE Transactions on Image Processing*, vol. 29, pp. 5862–5876, 2020.
- [21] M. Gharbi, J. Chen, J. T. Barron, S. W. Hasinoff, and F. Durand, "Deep bilateral learning for real-time image enhancement," *ACM Transactions on Graphics (TOG)*, vol. 36, no. 4, pp. 1–12, 2017.
- [22] W. Ren, S. Liu, L. Ma, Q. Xu, X. Xu, X. Cao, J. Du, and M.-H. Yang, "Low-light image enhancement via a deep hybrid network," *IEEE Transactions on Image Processing*, vol. 28, no. 9, pp. 4364–4375, 2019.
- [23] Y. Hu, H. He, C. Xu, B. Wang, and S. Lin, "Exposure: A white-box photo post-processing framework," *ACM Transactions on Graphics*, vol. 37, no. 2, pp. 1–17, 2018.
- [24] R. Wang, Q. Zhang, C.-W. Fu, X. Shen, W.-S. Zheng, and J. Jia, "Underexposed photo enhancement using deep illumination estimation," in *Proceedings of the IEEE Conference on Computer Vision and Pattern Recognition*, 2019, pp. 6849–6857.
- [25] R. Liu, L. Ma, J. Zhang, X. Fan, and Z. Luo, "Retinex-inspired unrolling with cooperative prior architecture search for low-light image enhancement," in *Proceedings of the IEEE/CVF Conference on Computer Vision and Pattern Recognition*, 2021, pp. 10 561–10 570.
- [26] W. Yang, S. Wang, Y. Fang, Y. Wang, and J. Liu, "From fidelity to perceptual quality: A semi-supervised approach for low-light image enhancement," in *the IEEE/CVF Conference on Computer Vision and Pattern Recognition*, 2020, pp. 3063–3072.
- [27] K. Xu, X. Yang, B. Yin, and R. W. Lau, "Learning to restore low-light images via decomposition-and-enhancement," in *Proceedings of the IEEE/CVF Conference on Computer Vision and Pattern Recognition*, 2020, pp. 2281–2290.
- [28] J. Li, X. Feng, and Z. Hua, "Low-light image enhancement via progressive-recursive network," *IEEE Transactions on Circuits and Systems for Video Technology*, vol. 31, no. 11, pp. 4227–4240, 2021.
- [29] Z. Xia, M. Gharbi, F. Perazzi, K. Sunkavalli, and A. Chakrabarti, "Deep denoising of flash and no-flash pairs for photography in low-light environments," in *the IEEE/CVF Conference on Computer Vision and Pattern Recognition*, 2021, pp. 2063–2072.
- [30] J. Cai, S. Gu, and L. Zhang, "Learning a deep single image contrast enhancer from multi-exposure images," *IEEE Transactions on Image Processing*, vol. 27, no. 4, pp. 2049–2062, 2018.
- [31] B. Moseley, V. Bickel, I. G. López-Francos, and L. Rana, "Extreme low-light environment-driven image denoising over permanently shadowed lunar regions with a physical noise model," in *Proceedings of the IEEE/CVF Conference on Computer Vision and Pattern Recognition*, 2021, pp. 6317–6327.
- [32] Y.-S. Chen, Y.-C. Wang, M.-H. Kao, and Y.-Y. Chuang, "Deep photo enhancer: Unpaired learning for image enhancement from photographs with gans," in *Proceedings of the IEEE Conference on Computer Vision and Pattern Recognition*, 2018, pp. 6306–6314.
- [33] J. Wang, W. Tan, X. Niu, and B. Yan, "Rdgan: Retinex decomposition based adversarial learning for low-light enhancement," in *Proceedings of IEEE International Conference on Multimedia and Expo*. IEEE, 2019, pp. 1186–1191.
- [34] K. Xu, H. Chen, C. Xu, Y. Jin, and C. Zhu, "Structure-texture aware network for low-light image enhancement," *IEEE Transactions on Circuits and Systems for Video Technology*, 2022.
- [35] L. Ma, T. Ma, R. Liu, X. Fan, and Z. Luo, "Toward fast, flexible, and robust low-light image enhancement," *arXiv preprint arXiv:2204.10137*, 2022.
- [36] G. K. Wallace, "The jpeg still picture compression standard," *IEEE transactions on consumer electronics*, vol. 38, no. 1, pp. xviii–xxxiv, 1992.
- [37] A. Skodras, C. Christopoulos, and T. Ebrahimi, "The jpeg 2000 still image compression standard," *IEEE Signal Processing Magazine*, vol. 18, no. 5, pp. 36–58, 2001.
- [38] T. Wiegand, G. J. Sullivan, G. Bjontegaard, and A. Luthra, "Overview of the h. 264/avc video coding standard," *IEEE Transactions on Circuits and Systems for Video Technology*, vol. 13, no. 7, pp. 560–576, 2003.
- [39] C. Zhao, J. Zhang, S. Ma, X. Fan, Y. Zhang, and W. Gao, "Reducing image compression artifacts by structural sparse representation and quantization constraint prior," *IEEE Transactions on Circuits and Systems for Video Technology*, vol. 27, no. 10, pp. 2057–2071, 2016.
- [40] Y. Kim, J. W. Soh, J. Park, B. Ahn, H.-S. Lee, Y.-S. Moon, and N. I. Cho, "A pseudo-blind convolutional neural network for the reduction of compression artifacts," *IEEE Transactions on Circuits and Systems for Video Technology*, vol. 30, no. 4, pp. 1121–1135, 2019.
- [41] Z. Jin, M. Z. Iqbal, W. Zou, X. Li, and E. Steinbach, "Dual-stream multi-path recursive residual network for jpeg image compression artifacts reduction," *IEEE Transactions on Circuits and Systems for Video Technology*, vol. 31, no. 2, pp. 467–479, 2020.
- [42] X. Fu, X. Wang, A. Liu, J. Han, and Z.-J. Zha, "Learning dual priors for jpeg compression artifacts removal," in *Proceedings of the IEEE/CVF International Conference on Computer Vision*, 2021, pp. 4086–4095.
- [43] D. P. Kingma and M. Welling, "Auto-encoding variational bayes," *arXiv preprint arXiv:1312.6114*, 2013.
- [44] J. Johnson, A. Alahi, and L. Fei-Fei, "Perceptual losses for real-time style transfer and super-resolution," in *Proceedings of European Conference on Computer Vision*. Springer, 2016, pp. 694–711.
- [45] X. Mao, Q. Li, H. Xie, R. Y. Lau, Z. Wang, and S. Paul Smolley, "Least squares generative adversarial networks," in *Proceedings of the IEEE International Conference on Computer Vision*, 2017, pp. 2794–2802.
- [46] L.-C. Chen, G. Papandreou, I. Kokkinos, K. Murphy, and A. L. Yuille, "Deeplab: Semantic image segmentation with deep convolutional nets, atrous convolution, and fully connected crfs," *IEEE Transactions on Pattern Analysis and Machine Intelligence*, vol. 40, no. 4, pp. 834–848, 2017.
- [47] B. C. Russell, A. Torralba, K. P. Murphy, and W. T. Freeman, "Labelme: a database and web-based tool for image annotation," *International Journal of Computer Vision*, vol. 77, no. 1, pp. 157–173, 2008.
- [48] J. Hai, Z. Xuan, R. Yang, Y. Hao, F. Zou, F. Lin, and S. Han, "R2rnet: Low-light image enhancement via real-low to real-normal network," *arXiv preprint arXiv:2106.14501*, 2021.
- [49] A. Aakerberg, K. Nasrollahi, and T. B. Moeslund, "RELLISUR: A real low-light image super-resolution dataset," in *Thirty-fifth Conference on Neural Information Processing Systems Datasets and Benchmarks Track*, 2021.
- [50] H. Bay, A. Ess, T. Tuytelaars, and L. Van Gool, "Speeded-up robust features (surf)," *Computer Vision and Image Understanding*, vol. 110, no. 3, pp. 346–359, 2008.
- [51] Z. Zhao, B. Xiong, L. Wang, Q. Ou, L. Yu, and F. Kuang, "Retinexdip: a unified deep framework for low-light image enhancement," *IEEE Transactions on Circuits and Systems for Video Technology*, 2021.
- [52] Y. Wang, R. Wan, W. Yang, H. Li, L.-P. Chau, and A. C. Kot, "Low-light image enhancement with normalizing flow," in *AAAI Conference on Artificial Intelligence*, 2022.
- [53] B. Lim, S. Son, H. Kim, S. Nah, and K. Mu Lee, "Enhanced deep residual networks for single image super-resolution," in *Proceedings of the IEEE conference on Computer Vision and Pattern Recognition Workshops*, 2017, pp. 136–144.
- [54] C. Yim and A. C. Bovik, "Quality assessment of deblocked images," *IEEE Transactions on Image Processing*, vol. 20, no. 1, pp. 88–98, 2010.
- [55] X. Tang, D. K. Du, Z. He, and J. Liu, "Pyramidbox: A context-assisted single shot face detector," in *Proceedings of the European conference on computer vision*, 2018, pp. 797–813.
- [56] S. Yang, P. Luo, C. C. Loy, and X. Tang, "Wider face: A face detection benchmark," in *Proceedings of the IEEE/CVF Conference on Computer Vision and Pattern Recognition*, 2016.